AUTHOR QUERIES

DATE 2/29/2012
JOB NAME WNP

ARTICLE 200508
QUERIES FOR AUTHORS K. Vedala et al.

THIS QUERY FORM MUST BE RETURNED WITH ALL PROOFS FOR CORRECTIONS

AU1) Please check the running head introduced.
AU2) Please consider separating the section "Results and Discussion."
AU3) Please provide manufacturer name and location of "CASCADE."
AU4) Please provide chapter title and publisher location for the reference "Taylor et al., 1994."
AU5) Please provide article editors name and location for the reference "Tong et al., 1990."
AU6) Please note that Tables 2 A and B were considered as Tables 2 and 3, respectively, and subsequent table was renumbered accordingly. Please check.

Peak Detection of Somatosensory Evoked Potentials Using an Integrated Principal Component Analysis–Walsh Method

Krishnatej Vedala, Ilker Yaylali,† Mercedes Cabrerizo,* Mohammed Goryawala,* and Malek Adjouadi**

Summary: Clinical application of somatosensory evoked potentials (SSEP) in intraoperative neurophysiological monitoring still requires anywhere between 200 to 500 trials, which is excessive and introduces a delay during surgery. In this study, the analysis was performed on the data recorded in 20 patients undergoing surgery during which the posterior tibial nerve was stimulated and SSEP response was recorded from scalp. The first 10 trials were analyzed using an eigen decomposition technique, and a signal extraction algorithm eliminated the common components of the signals not contributing to the SSEP. A unique Walsh transform operation was then used to identify the position of the SSEP event within the clinical requirements of 10% time in latency deviation and 50% peak-to-peak amplitude deviation using only 10 trials. The algorithm also shows consistency in the results in monitoring SSEP in up to 6-hour surgical procedures even under this significantly reduced number of trials.

Key Words: Somatosensory evoked potentials, Eigen decomposition, Walsh transform, SSEP detection.

(*J Clin Neurophysiol* 2012;0: 1–9)

Somatosensory evoked potential (SSEP) monitoring is an integral part of most of the present day spinal surgeries. This involves monitoring of the P37 and N45 peaks of the bipolar EEG recordings from their initial value (called baseline value) throughout the surgical procedure. The primary difficulty ever since the concept was introduced has been to improve the signal-to-noise ratio (SNR) of the readings. A simple but powerful signal averaging method was introduced (Dawson, 1947) to improve the SNR by $\sqrt{N}$, where N is the number of signals (trials). The shortcomings of this method however can be summarized as follows:

1. The SNR of raw SSEP signal is very low requiring a large value for N varying from 200 to 500 per subject (Regan, 1990); and
2. a larger value of N would require more time to identify the SSEP event.

As a consequence, the approach taken in this study is to expedite the detection of SSEP with an optimal number of trials (limited to 10 in this case) that will ultimately allow for timely decision by the surgeons.

The signal averaging approach remains the most prevalent method for intraoperative neurophysiological monitoring (Hussain, 2008), and a faster approach of recording SSEP signals would make spinal surgeries safer (Taylor et al., 1994). Current systems rely on peak detection or area under the SSEP curve (Taylor et al., 1994) for automating the SSEP detection. There is a need for better algorithms that minimize these unyielding numbers of trials and are able to remove automatically those signals that are fraught with noise.

A first approach that addressed the issue of decreasing the number of trials is based on a parametric decomposition of SSEP signals (Bai et al., 2001), which was later revisited using Bayesian analysis (Truccolo et al., 2003). Another approach involved the use of amplitude modulated stimulus and performing steady-state analysis on the recorded signals (Noss et al., 1996). The latency, that is, the time difference between the successive trials, was also exploited for noise removal (Kong and Oiu, 2001). Recent advances in functional source separation of SSEP signals (Porcaro et al., 2009) provide better insight into the EEG signal characteristics that can be used for SSEP signal detection. Artificial neural network processing has been used successfully to classify auditory evoked potentials and to classify anesthetic states but still requiring 1,000 trials (Zhang et al., 2001). A phase-based technique (Simpson et al., 2000) designed to improve this averaging rate reduced successfully this number to 200 trials. An improved SSEP recording scheme has been proposed (MacDonald et al., 2005) that can improve the SNR drastically and a rapid recording can be obtained.

The approach proposed in this study reduces this average to an optimal number of 10 trials using an eigen-decomposition technique coupled with a unique Walsh operator that is able to pinpoint the position of maximum amplitude, which serve as an indicator of the presence of SSEP. A measure of caution is taken, in that a thorough mathematical assessment of the eigen components is performed at the onset to remove any trial that is fraught with noise in order not to burden the averaging process with the intention not to exceed 10 trials as a maximum. In the clinical cases involved in this study, with a stimulus rate of 3.1 Hz, using 200 to 500 trials, the time required to record the trials varies anywhere between 1 minute and 3 minutes. Standard algorithms often consider time–amplitude variations between individual trials and common features between the individual signals. The later fact led to the use of the principal component analysis (PCA) for estimating components associated with noise (Glaser and Ruchkin, 1976; Moore, 1981; Regan, 1990; Suter, 1970). The PCA is based on eigen decomposition of the raw SSEP signal matrix. A modified version of PCA-based signal decomposition technique named Algorithm for Multiple Signal Extraction (AMUSE) (Crespo-Garcia et al., 2008; Tong et al., 1990) is used to reduce the number of trials to 10. Walsh transform is implemented such as to automate the latency detection after the SSEP signal is obtained. The

From the *Center for Advanced Technology and Education, College of Engineering and Computing, Florida International University, Miami, Florida, U.S.A.; and †Department of Clinical Neurophysiology, Oregon Health & Science University, Portland, Oregon, U.S.A.

The experimental work of this study was carried out under the support of IRB#052708-03 and IRB#100410-00, and collected data as a routine part of a spine surgery were deidentified at the source.

Address correspondence and reprint requests to Malek Adjouadi, PhD, Center for Advanced Technology and Education, College of Engineering & Computing, Florida International University, 10555 W. Flagler Street, EC 2672, Miami, FL 33174, U.S.A.; e-mail: adjouadi@fiu.edu.

ISSN: 0736-0258/12/0000-0001

broad scope of applicability of the Walsh transform yielded, as examples, excellent results in (1) extracting stereo features to recover depth information in 2-dimensional images (Adjouadi and Candocia, 1994; Adjouadi et al., 1996; Candocia and Adjouadi, 1997) and (2) detecting interictal spikes in EEG data as a means to detect seizures in pediatric epilepsy (Adjouadi et al., 2004, 2005; Tito et al., 2010). In this SSEP application, a second-order Walsh operator has shown to be extremely effective in localizing the SSEP under only 10 trials even when the morphology of this signal is not yet quite similar as that of the morphology expected with a larger number of trials (200–500).

METHOD

Structure of the Algorithm

[F1] The structure of the proposed algorithm is illustrated in Figure 1 and explanations for each step are as follows:

1. The original data matrix, which certainly includes noisy signals, is generated using recorded SSEP signals during successive trials from the same bipolar recording channel spanning the rows

$$X = \begin{bmatrix} x_1(1) & x_2(1) & \cdots & x_m(1) \\ x_1(2) & x_2(2) & \cdots & x_m(2) \\ \vdots & \vdots & \ddots & \vdots \\ x_1(n) & x_2(n) & \cdots & x_m(n) \end{bmatrix} = \begin{bmatrix} x(1)^T \\ x(2)^T \\ \vdots \\ x(n)^T \end{bmatrix},$$

where $X(n) = [\, x_1(n) \quad x_2(n) \quad \cdots \quad x_m(n) \quad \cdots \quad x_M(n) \,]^T$ is the nth trial data, $x(n)$ is the vector of nth trial and $x_m(n)$ is the mth sample from nth trial data.

2. The AMUSE algorithm (Crespo-Garcia et al., 2008; Tong et al., 1991), similar to the PCA, is applied on the matrix X following the steps below:
   (a) Compute the $N \times N$ covariance matrix: $R_x = X.X^T$
   (b) Determine the singular values Φ of R_x using singular value decomposition technique giving three matrices: U is a unitary matrix, V is a diagonal matrix for transformation, and Φ is the required matrix: $R_x = V.\Phi.U$

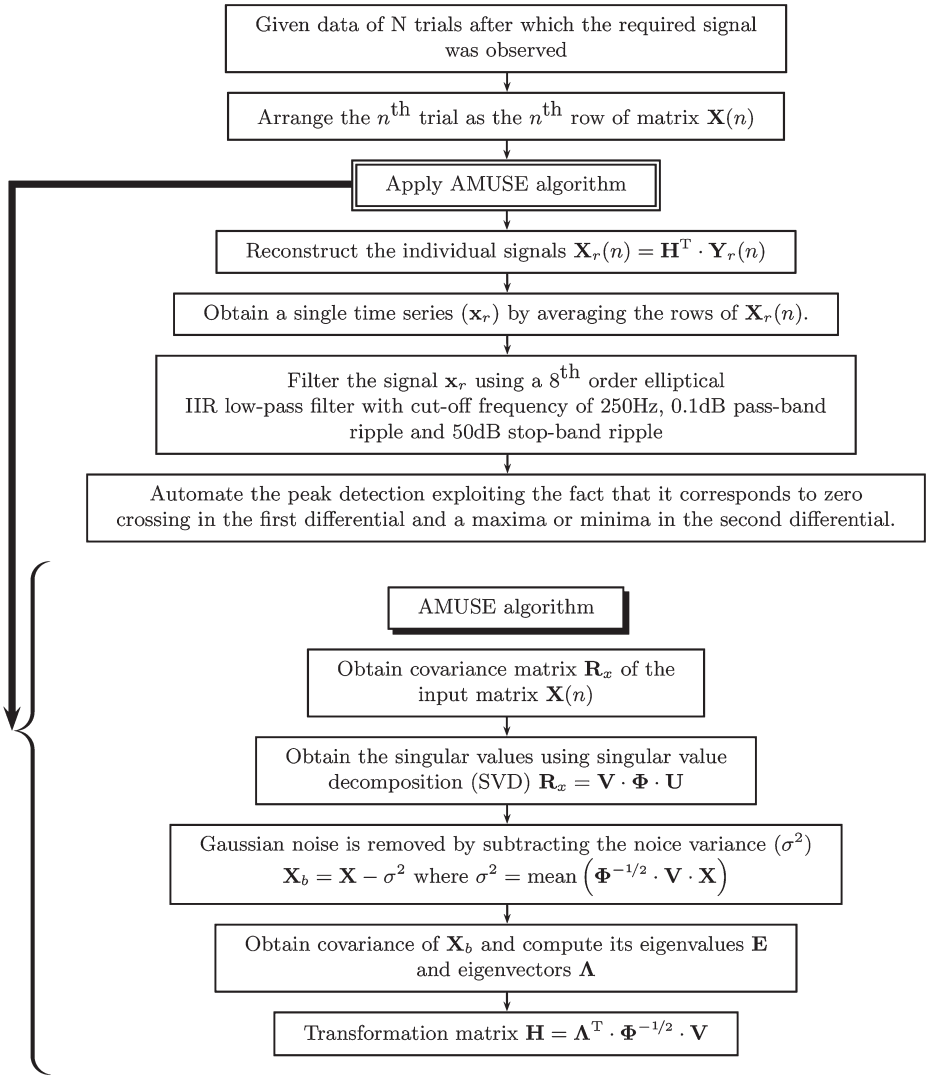

FIG. 1. Flowchart for the algorithm discussed is displayed in the left column and the details of AMUSE algorithm below it are indicated by the arrow.

(c) Remove the Gaussian noise components by subtracting the noise variance estimated as the mean of the singular matrix with the equation $\sigma^2 = \text{mean}\left(\Phi^{-\frac{1}{2}} \cdot V \cdot X\right)$ such that $X_b = X - \sigma^2$
(d) Determine the covariance of X_b and further decompose it to find its eigenvalues and the corresponding eigenvectors Λ to be used in the next step. This step ensures that all the singular values are distinct.
(e) Obtain the transformation matrix $H = \Lambda^T \cdot \Phi^{-\frac{1}{2}} \cdot V$
(f) Determine the independent components as $Y(n) = H.X$.

3. Individual components were then studied and those that had the difference between first 2 consecutive frequency peaks less than −30 dB/Hz were removed. To remove a component, the corresponding row of $Y(n)$ was replaced with zeros and a new matrix $Y_r(n)$ was consequently constructed.
4. New individual signals as rows of X were then retrieved from the matrix $Y(n)$ obtained in the previous step using the equation: $X_r(n) = H^T \cdot Y_r(n)$
5. Arithmetic mean was computed across each column to obtain a single time varying signal and was passed through a 250 Hz low-pass filter, for experimental reasons that are detailed in the implementation section.
6. Detection of the peak that coincides with the occurrence of the SSEP was automated using the Walsh transformation method (Adjouadi et al., 2004, 2005; Smith, 1981; Weide et al., 1978) to indicate the evoked potential response.

In retrospect, the AMUSE algorithm is equivalent to cascading two PCA systems (Tong et al., 1991), with the following basic assumptions:

- Data is a set of zero-mean wide-sense ergodic process, the components of which are mutually independent.
- Noise in the data is assumed zero-mean white Gaussian noise.

Implementation

[F2] As an illustrative example, Figure 2 shows comparative results of the algorithm using 10 trials for a subject in contrast with the results obtained using the conventional method with 200 trials. MATLAB programs were created by the authors that take the raw signal vector and the possible number of components as input and returns the estimated components, the transformation matrix, and reconstructed signals as the output. Once the components are estimated, filtering is used to remove unwarranted components.

The present study involved initially 16 subjects with the objective to estimate the location of the SSEP event using only 10 trials in comparison with the locations provided by clinical experts using 200 to 500 trials, and 4 other subjects were later included in the study with recordings provided at different stages of their respective surgical procedures. These last data sets were assessed to ascertain consistency and reproducibility of the results in time latencies and peak-to-peak amplitudes. For the recording process, two bipolar channels C_3-C_4 and C_Z-F_Z were used to record the desired signals. The SSEP signals were recorded by applying stimuli of intensity 45 mA and pulse duration of 200 microseconds at the posterior tibial nerve of the right leg with a 3.1-Hz repetition rate. The positive terminal of stimulus is connected to the distal end, and the negative terminal to the proximal end of the tibial nerve. The amplifier gain was set to 10, and a 25 μV trial rejection threshold is used. The data were recorded at 6,400 Hz sampling rate for a duration of 100 milliseconds and with the 60 Hz external interference component

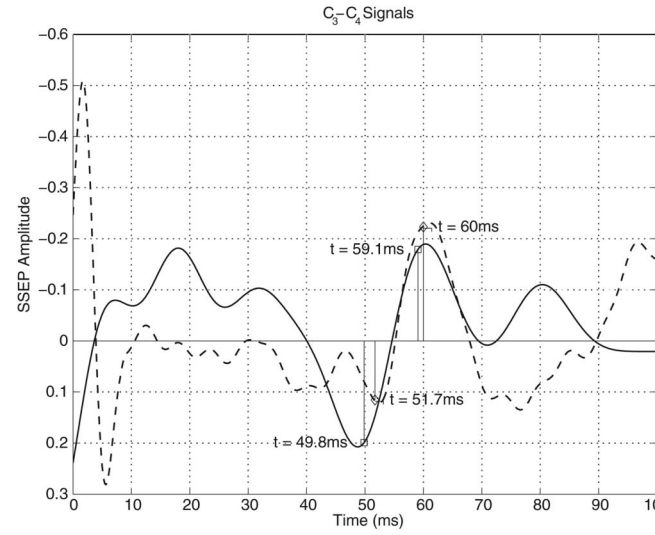

FIG. 2. Comparison between the results of the algorithm using 10 trials (solid line) and the clinical data using 200 trials (dotted line). Time instances shown to the left of the markers are the locations where the evoked potential was detected using the Walsh transformation method on C_3-C_4 signal. The time values on the right hand side of the markers are the time instances of the SSEP selected by clinical experts.

removed, yielding 640 samples per signal. The raw trial signals are band limited from 10 to 1,000 Hz, and the clinical average was between 30 and 500 Hz. For illustration purposes, the 10 resulting independent components in one of the studies are shown in Figure 3 with similar results obtained for the other recording channel. From these plots, it is evident that the higher eigenvectors are the ones representing the low-frequency components. [F3]

AMUSE Algorithm—Noise Components Filtering

An important observation was that the lower eigenvalue components had very sharp power peaks at single frequency and the higher eigenvalue components had sharp spikes at multiple frequencies. The cause can be attributed to the statistical variance exhibited by the higher magnitude eigenvalues.

It can be inferred that because these singular frequency components will contribute solely to their corresponding frequencies, they can be eliminated. For reconstruction purposes, the components that have less than 2 peaks higher than −30 dB/Hz were removed. The −30 dB/Hz threshold was arbitrarily chosen based on the total power contribution of the component. To show the significance of the observation, raw data from the first 10 trials are averaged in time compared with the average of 200 trials from the same subject during the same operation; the low-frequency components were estimated and removed, and a final signal was obtained as shown in Figure 4. [F4]

It should be indicated that the signal obtained after filtering is still not smooth enough to obtain a valid inference. The average signal obtained was filtered using an eighth-order Butterworth low-pass filter with a cutoff frequency of 250 Hz. The signal was then tested for the maxima and minima using the first-order and second-order differentials. The peaks in the Walsh-transformed signal are then used to automate the identification of the evoked response. A difference operator can be used, but they have a serious drawback of being highly susceptible to noise and a smoothing operator has to

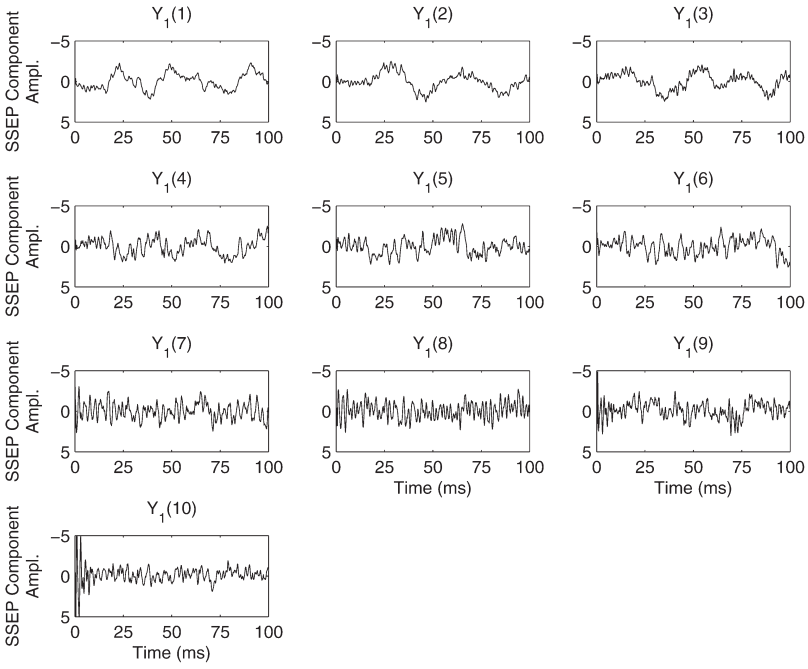

FIG. 3. $Y_1(n)$. The 10 components of the 10 trials recorded (X_1 (n)) from the C_Z-F_Z channel and decomposed using AMUSE algorithm. The x-axis represents the sampling time intervals, and the y-axis represents the amplitude of these components.

be involved to improve the differentiator's SNR. The Walsh differentiation method (Adjouadi et al., 2004, 2005) was used to overcome the problem, as described below.

Walsh Transform—Automated Peak Detection

The second-order Walsh operator of length 4 ($w_N^r = w_4^2$), equivalent to a 4-point second-order differentiation operator, was convolved with the average signal to obtain a Walsh-transformed signal whose peak location is found to determine the peak locations of the SSEP (at least for 70% of the cases where noise was not preponderant). The magnitude of each of the points as a function of time of this Walsh-transformed signal was defined by performing the following convolution:

$$W = \frac{1}{4}\left(w_4^2 * X_{\text{final}}\right),$$

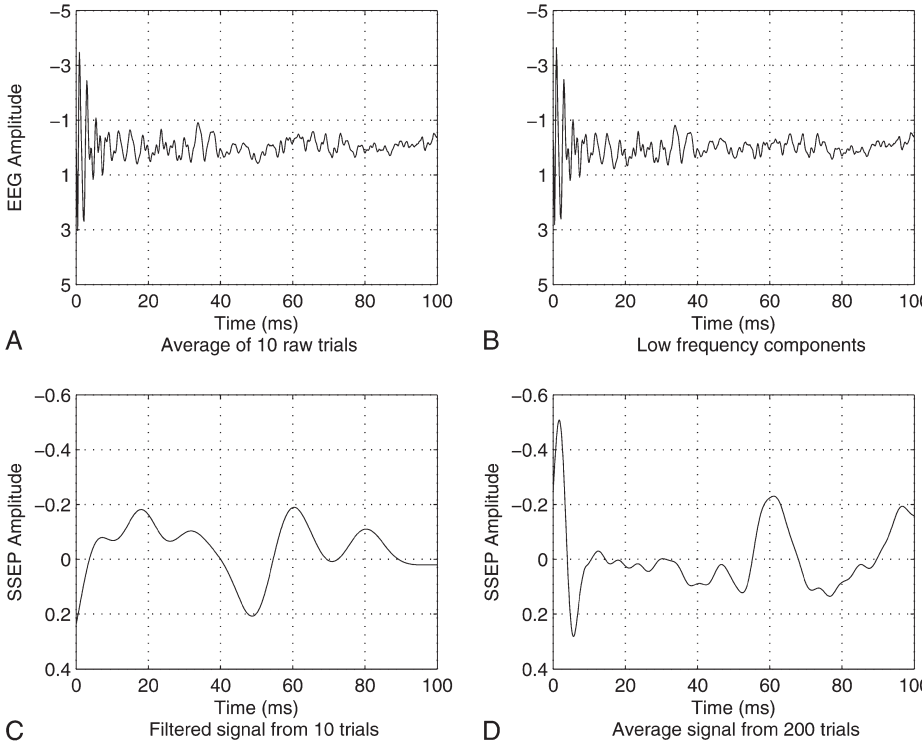

FIG. 4. Significance of removing the low-frequency components: **A**, Average of raw signals from 10 trials. **B**, Noise components estimated from the 10 trials in Figure 3. Average of raw signals from 200 trials (**C**) and signal obtained after filtering signal in **A** (**D**), showing the possible location of the SSEP response. The x-axis represents the time in seconds.

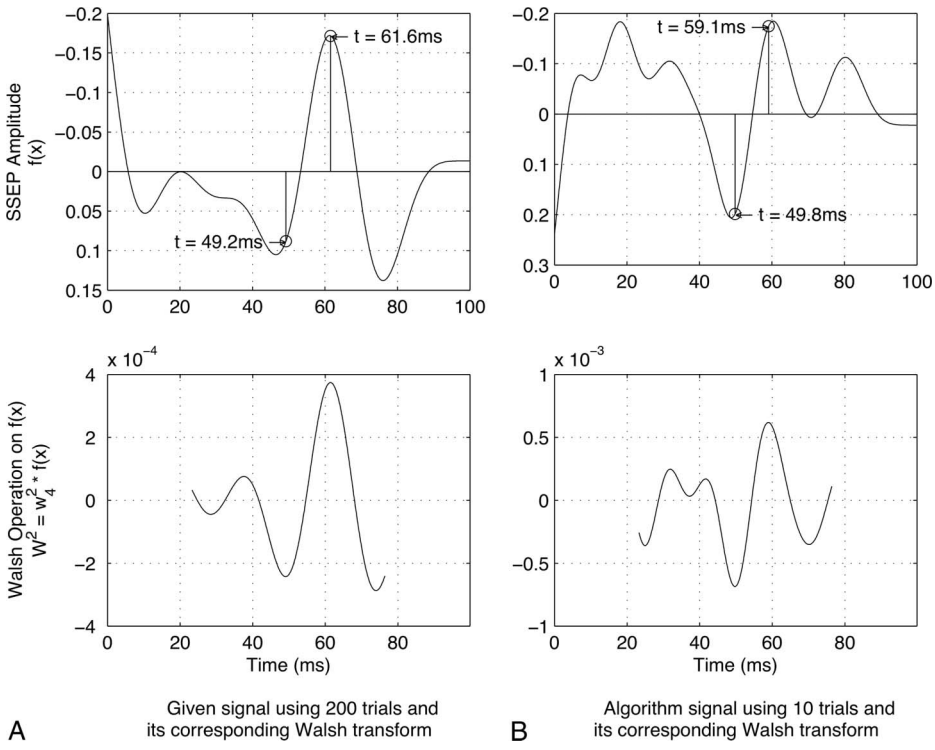

FIG. 5. Application of Walsh transform to identify the position of the SSEP: **A**, Left column displays the signal obtained using conventional averaging. The plot on the top left shows the given average signal obtained from 200 trials, and the possible location of evoked potential response using the Walsh operation is shown below it. **B**, Right column displays the signal obtained using the proposed algorithm, and the detected location of evoked potential response obtained using the Walsh operation is shown below it.

where $w_4^2 = [1 \quad -1 \quad -1 \quad 1]$ is the Walsh kernel, which is functionally similar to the second-order derivative and the center point difference [1 −2 1], and where the symbol "*" represents the convolution operation. The peaks of W are obtained to localize the two peaks of the SSEP response corresponding to P37 and N45 for the tibial nerve. The Walsh maximum always corresponds to either P37 or N45 that is verified from the sign of the amplitude of the signal at the detected time instance. Once the maximum peak is obtained automatically, the next maximum point with opposite polarity defines the second peak.

Figure 5 shows the process as it applies for subject 2, and as can be seen, the method effectively filters the noise and highlights the evoked response with just 10 trials. The figure compares the time occurrence of Walsh-transformed peaks detected on the given average signal in Figure 5A with that from the signal obtained from 10 trials using the proposed algorithm in Figure 5B. The algorithm [F5]

TABLE 1. Result Analysis of the Algorithm Implementation in Detecting the SSEP Locations for 16 Subjects

Subject Number	No. Trials	C_3-C_4 Peak Latencies (Millisecond)				C_Z-F_Z Peak Latencies (Millisecond)				Difference Between Clinical and Algorithm Latencies (Millisecond)			
		Clinical		Algorithm		Clinical		Algorithm		C_3-C_4		C_Z-F_Z	
		P37	N45	P37	N45	P37	N45	P37	N45	P37	N45	P37	N45
1	196	35.0	45.0	31.4	38.4	43.0	58.0	46.9	58.6	3.6	6.6	3.9	0.6
2	100	38.0	50.0	45.8	57.2	30.0	40.0	38.8	46.2	7.8	7.2	8.8	6.2
3	34	45.0	57.0	45.0	55.8	47.0	56.0	39.2	46.2	0.0	1.2	7.8	9.8
4	102	45.0	57.0	45.0	56.2	35.0	47.0	36.6	46.8	0.0	0.8	1.6	0.2
5	200	42.0	53.0	38.4	49.2	44.2	52.0	44.2	51.1	3.6	3.8	0.0	0.9
6	227	43.4	51.7	38.8	50.3	44.2	52.0	41.1	52.7	4.6	1.4	3.1	0.7
7	230	40.4	47.6	36.7	49.7	40.6	48.7	48.0	61.4	3.7	2.1	7.4	12.7
8	237	51.4	60.3	45.2	52.0	53.1	60.0	43.4	50.2	6.2	8.3	9.7	9.8
9	221	42.1	50.3	46.1	53.0	43.2	51.5	49.1	58.0	4.0	2.7	5.9	6.5
10	229	43.7	50.4	48.8	54.8	46.4	51.8	41.6	51.4	5.1	4.4	4.8	0.4
11	214	45.0	55.3	50.9	58.4	46.4	56.0	52.2	67.3	5.9	3.1	5.8	11.3
12	236	36.6	40.9	36.4	48.0	40.4	47.9	46.4	58.0	0.2	7.1	6.0	10.1
13	234	38.7	49.0	40.6	47.5	48.1	56.0	46.1	53.3	1.9	1.5	2.0	2.7
14	228	41.7	48.2	50.2	57.3	42.3	53.4	44.2	51.3	8.5	9.1	1.9	2.1
15	225	40.9	47.9	41.9	48.8	41.2	50.0	44.1	51.1	1.0	0.9	2.9	1.1
16	225	35.0	40.0	37.3	44.4	35.0	56.8	51.7	58.8	2.3	4.4	16.7	2.0
								Average		3.7	4.0	5.5	4.8

TABLE 2. Algorithm Consistency Analysis on 3 Subjects (Numbers 17, 18, and 19) Recorded at Different Time Intervals During the Respective Surgeries

AQ : 6

Subject Number	Time of Recording	C_3-C_4 Peak Latencies (Millisecond)				C_Z-F_Z Peak Latencies (Millisecond)			
		Clinical		Algorithm		Clinical		Algorithm	
		P37	N45	P37	N45	P37	N45	P37	N45
17	10:24 AM	40.6	50.3	43.3	47.5	40.0	49.5	38.1	45.2
	11:01 AM	41.2	60.0	40.5	47.5	41.0	60.0	40.5	48.3
	11:30 AM	40.1	56.4	46.7	53.3	40.7	49.2	39.2	55.8
	11:56 AM	37.5	60.0	40.0	45.5	40.6	48.9	38.8	46.2
	12:22 PM	40.7	47.1	39.1	45.6	40.3	49.3	38.8	45.2
18	8:45 AM	51.4	58.4	49.8	59.2	50.3	58.1	45.5	53.3
	9:49 AM	51.5	61.0	55.3	63.0	50.9	51.2	48.4	56.1
	10:13 AM	51.7	60.0	47.2	58.1	50.6	59.0	52.0	58.9
	10:24 AM	52.5	61.0	55.0	62.5	50.3	59.0	45.0	52.5
	10:32 AM	51.7	60.3	51.3	56.7	50.3	58.4	54.5	61.2
19	4:00 PM	40.6	48.7	49.8	57.8	41.8	48.4	39.4	46.6
	5:00 PM	41.5	50.1	45.0	52.0	42.8	46.5	40.8	47.5
	5:57 PM	41.5	49.8	45.9	53.4	41.7	50.6	38.8	45.9

Subject Number	% Interset Variation From the First Recording Set Per Subject								Difference Between Clinical and Algorithm Latencies (Millisecond)			
	C_3-C_4				C_Z-F_Z				C_3-C_4		C_Z-F_Z	
	Clinical		Algorithm		Clinical		Algorithm					
	P37	N45	P37	N45	P37	N45	P37	N45	P37	N45	P37	N45
17	—	—	—	—	—	—	—	—	2.7	2.8	1.9	4.3
	1.5%	19.3%	6.5%	0.0%	2.5%	21.2%	6.3%	6.9%	0.7	12.5	0.5	11.7
	1.2%	12.1%	7.9%	12.2%	1.8%	0.6%	2.9%	23.5%	6.6	3.1	1.5	6.6
	7.6%	19.3%	7.6%	4.2%	1.5%	1.2%	1.8%	2.2%	2.5	14.5	1.8	2.7
	0.2%	6.4%	9.7%	4.0%	0.7%	0.4%	1.8%	0.0%	1.6	1.5	1.5	4.1
18	—	—	—	—	—	—	—	—	1.6	0.8	4.8	4.8
	0.2%	4.5%	11.0%	6.4%	1.2%	11.9%	6.4%	5.3%	3.8	2	2.5	4.9
	0.6%	2.7%	5.2%	1.9%	0.6%	1.5%	14.3%	10.5%	4.5	1.9	1.4	0.1
	2.1%	4.5%	10.4%	5.6%	0.0%	1.5%	1.1%	1.5%	2.5	1.5	5.3	6.5
	0.6%	3.3%	3.0%	4.2%	0.0%	0.5%	19.8%	14.8%	0.4	3.6	4.2	2.8
19	—	—	—	—	—	—	—	—	9.2	9.1	2.4	1.8
	2.2%	2.9%	9.6%	10.0%	2.4%	3.9%	3.6%	1.9%	3.5	1.9	2	1
	0.0%	0.6%	1.8%	2.4%	2.6%	8.5%	5.1%	3.4%	4.4	3.6	2.9	4.7
							Average		2.7	4.4	2.5	4.9

For the results to be consistent, the peak latencies should be within 10% of the first peak (baseline value) throughout the surgery in at least one electrode as highlighted.

was successfully implemented on 20 subjects ensuring the repeatability of the algorithm.

AQ : 2

RESULTS AND DISCUSSIONS

The details on the trials and SSEP locations of the 20 subjects included in the study are summarized in Tables 1–4. For each of the first 16 subjects, Table 1 provides the SSEP response locations for the two bipolar recording channels obtained clinically and are contrasted to those locations determined by the proposed algorithm. It includes the error (difference) in milliseconds of the estimated SSEP location with respect to the corresponding actual location as provided by the clinicians. For 14 of these 16 subjects, the location determined by the proposed algorithm relied solely on the first 10 trials or recorded signals. For the remaining 2 subjects, it was noted that 2 of the first 10 trials were corrupted and were replaced by the successively recorded signals to constitute the required 10 trials, for consistency purposes.

1 – T4]

With the initial findings in using these 16 subjects, 4 more subjects were added to the study to assess consistency in detecting the baseline peak latencies. To prove the plausibility of an SSEP monitoring system, the system should show consistency at different times in a single surgical procedure. Four such cases were then obtained and analyzed for at least one consistent peak throughout the procedure. The highlighted entries show the consistency of the peaks, that is, within $\pm 10\%$ of the first peak latency (baseline value) as detected by the algorithm using 10 trials. Tables 2 and 3 show time latencies for the 4 surgeries, and Table 4 provides the peak-to-peak amplitudes for the subjects in Tables 2 and 3. It can be observed that for the channels in which the time latencies were found consistent, the amplitudes were found to be consistent within 50% variation from the respective baseline values.

TABLE 3. Algorithm Consistency Analysis for Subject 20 at Different Instances During a 6-Hour Surgical Procedure

Subject Number	Time of Recording	C_Z-F_Z Peak Latencies (Millisecond)				% Interset Variation From the First Recording Set Per Subject				Difference Between Clinical and Algorithm Latencies (Millisecond)	
		Clinical		Algorithm		Clinical		Algorithm			
		P37	N45	P37	N45	P37	N45	P37	N45	P37	N45
20	9:43 AM	49.8	58.9	45.9	54.2	—	—	—	—	3.9	4.7
	10:05 AM	50.3	58.1	47.7	55.6	1.0%	1.4%	3.9%	2.6%	2.6	2.5
	10:30 AM	50.1	59.0	50.3	57.0	0.6%	0.2%	9.6%	5.2%	0.2	2.0
	10:55 AM	50.1	58.1	46.7	59.2	0.6%	1.4%	1.7%	9.2%	3.4	1.1
	11:28 AM	48.4	57.3	45.8	58.1	2.8%	2.7%	0.2%	7.2%	2.6	0.8
	11:50 AM	47.9	56.8	44.8	52.8	3.8%	3.6%	2.4%	2.6%	3.1	4.0
	12:20 PM	47.1	56.7	41.9	48.0	5.4%	3.7%	8.7%	11.4%	5.2	8.7
	12:45 PM	47.0	56.0	45.9	58.8	5.6%	4.9%	0.0%	8.5%	1.1	2.8
	1:05 PM	47.3	55.6	41.4	48.4	5.0%	5.6%	9.8%	10.7%	5.9	7.2
	1:35 PM	45.6	55.1	44.7	51.6	8.4%	6.5%	2.6%	4.8%	0.9	3.5
	1:55 PM	46.7	55.6	46.2	59.8	6.2%	5.6%	0.7%	10.3%	0.5	4.2
	2:20 PM	45.7	55.2	47.3	54.2	8.2%	6.3%	3.1%	0.0%	1.6	1.0
	2:45 PM	47.1	55.7	49.4	57.3	5.4%	5.4%	7.6%	5.7%	2.3	1.6
	3:04 PM	46.2	55.4	45.0	51.9	7.2%	5.9%	2.0%	4.2%	1.2	3.5
	3:28 PM	46.0	54.8	41.6	60.8	7.6%	7.0%	9.4%	12.2%	4.4	6.0
	3:45 PM	45.9	55.0	46.6	54.2	7.8%	6.6%	1.5%	0.0%	0.7	0.8
								Average		2.5	3.4

Only the C_Z-F_Z recordings were clinically provided for analysis.

TABLE 4. Amplitude Consistency for Subjects 17 Through 20 Corresponding to the Peak Latencies Shown in Tables 2 and 3

Subject Number	Time of Recording	P-P Amplitude (μV)	P-P Amplitude Error (%)
17	10:24 AM	0.66	—
	11:01 AM	0.57	13
	11:30 AM	0.65	2
	11:56 AM	0.93	41
	12:22 PM	0.61	9
18	8:45 AM	0.53	—
	9:49 AM	0.28	47
	10:13 AM	0.46	12
	10:24 AM	0.50	5
	10:32 AM	0.63	19
19	4:00 PM	0.51	—
	5:00 PM	0.73	43
	5:57 PM	0.52	2
20	9:43 AM	0.91	—
	10:05 AM	0.86	5
	10:30 AM	0.70	23
	10:55 AM	0.62	32
	11:28 AM	0.48	47
	11:50 AM	0.65	28
	12:20 PM	0.85	6
	12:45 PM	0.82	10
	1:05 PM	1.00	10
	1:35 PM	0.74	18
	1:55 PM	0.51	44
	2:20 PM	0.66	27
	2:45 PM	0.70	23
	3:04 PM	0.87	4
	3:28 PM	0.92	2
	3:45 PM	0.74	18

For subjects 17, 19, and 20, the amplitudes are from C_Z-F_Z channel and for subject 18 from the C_3-C_4 channel.

It can be seen from Tables 1–4 and Figures 2 and 6 that the [F6] algorithm output from 10 trials using the proposed algorithm closely mimics (within a 10% time latency deviation and within 50% peak-to-peak amplitude deviation) the average signal obtained clinically using a multitude of trials, and the response could be clearly visualized. This algorithm is simple enough to be implemented in the recording device itself.

Present day recording systems, such as CASCADE Intraoperative Monitoring rely on amplitude threshold or area under the curve schemes for the SSEP peak detection. A well-defined criterion needs to be applied to appropriately remove the noisy trial recordings, and a much better response can be obtained while still contending with a limited number of trials. Another observation is that the individual trials show a typical frequency pattern wherein the average power density in the frequency range of 0 Hz to 50 Hz is at least 10 dB/Hz greater than that in the frequency range of 100 to 200 Hz. This information can be used to implement automated noisy signal elimination and to enhance the performance of the system. The algorithm implemented for all the subjects achieved very promising SSEP detection results with an accurate detection in at least one bipolar recording channel. AQ : 3

With all these results, a retrospective on the merits of the proposed algorithm helps us to

- identify and get rid of the corrupted SSEP signal components,
- determine the time (latency) variations in different SSEP trials, and
- justify our assumption of independent SSEP trial signals.

CONCLUSION

The eigen-decomposition process helped reduce significantly the number of trials, a clinical outcome that is highly desirable, and

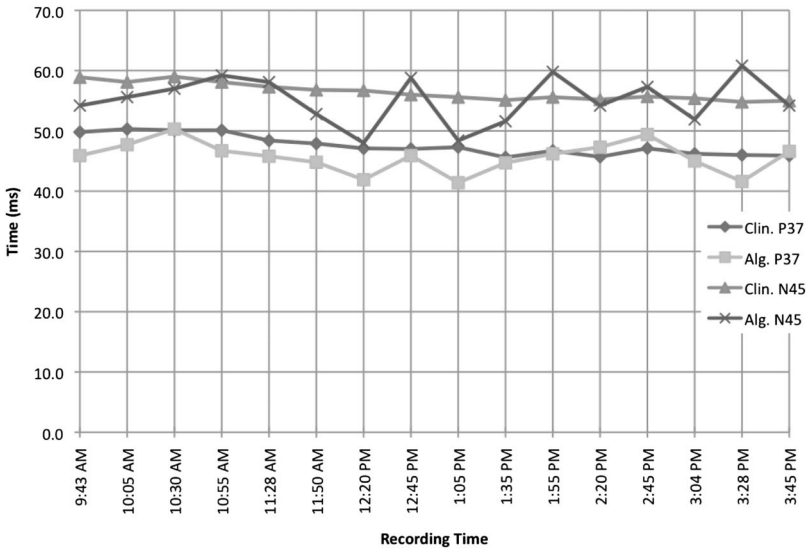

FIG. 6. Consistency in detecting P37 and N45 peak latencies from the C_Z-F_Z recording of subject 20 with the peak latencies (algorithm vs. clinical) as given in Table 4.

allowed for a thorough assessment that delineated signal trend from noise. The use of the Walsh operator proved highly effective in detecting the evoked potential peak latencies using an optimal number of trials (in this study, 10). The algorithm no longer depends on the signal morphology and automates the process from selection of a minimum number of trials based on their frequency response, applying the algorithm on them and using the unique Walsh transformation method to automatically indicate the SSEP response and the peak latencies. The results from the automated detection scheme and interpretation of the characteristic peak using the Walsh operation coincide with the opinions of the experts.

For all of the cases, the noted average misalignment between the clinical peak latencies and those obtained using the proposed algorithm, including both bipolar channels, was 3.38 and 4.3 milliseconds for P37 and N45, respectively. It should be stated that when such misalignments happen during a surgical procedure, even when a maximum number of trials is used, clinicians select one of the two channels that is viewed as more representative of the SSEP morphology.

The Walsh operator proved highly effective in identifying the SSEP occurrence even when the morphology of the signal is quite different from that obtained at a much higher number of trials. In the automated process, a thorough analysis yielded a better mathematical assessment of the noise signal involved in evoked potentials. Because there are no intensive mathematical operations involved in the algorithm, it can be feasibly realized in hardware form and/or integrated in the present systems, proving a very valuable tool in intraoperative neurophysiological monitoring.

ACKNOWLEDGMENTS

The authors appreciate the support provided by the National Science Foundation under grants CNS-0959985, HRD-0833093, and CNS-1042341. They are also thankful for the clinical support provided by the Department of Clinical Neurophysiology at the Oregon Health and Science University, the Ware Foundation, and the joint Neuro-Engineering Program between Florida International University and Miami Children's Hospital.

REFERENCES

Adjouadi M, Candocia F. A stereo matching paradigm based on the Walsh transformation. *IEEE Trans Pattern Anal Mach Intell* 1994;16:1212–1218.

Adjouadi M, Candocia F, Riley J. Exploiting Walsh-based attributes to stereo vision. *IEEE Trans Signal Process* 1996;44:409–420.

Adjouadi M, Cabrerizo M, Ayala M, et al. Detection of interictal spikes and artifactual data through orthogonal transformations. *J Clin Neurophysiol* 2005;22:53–64.

Adjouadi M, Sanchez D, Cabrerizo M, et al. Interictal spike detection using the Walsh transform. *IEEE Trans Biomed Eng* 2004;51:868–872.

Bai O, Nakamura M, Nagamine T, Shibasaki H. Parametric modeling of somatosensory evoked potentials using discrete cosine transform. *IEEE Trans Biomed Eng* 2001;48:1347–1351.

Candocia F, Adjouadi M. A similarity measure for stereo feature matching. *IEEE Trans Image Process* 1997;6:1460–1464.

Crespo-Garcia M, Atienza M, Cantero JL. Muscle artifact removal from human sleep EEG by using independent component analysis. *Ann Biomed Eng* 2008;36:467–475.

Dawson GD. Cerebral responses to electrical stimulation of peripheral nerve in man. *J Neurol Neurosurg Psychiatry* 1947;10:134–140.

Glaser E, Ruchkin DS. *Principles of neurobiological signal analysis*. New York: Academic Press, 1976.

Hussain AM, ed. *A practical approach to neurophysiologic intraoperative monitoring*. New York: Demos Medical Publishing, 2008.

Kong X, Oiu T. Latency change estimation for evoked potentials: a comparison of algorithms. *Med Biol Eng Comput* 2001;39:208–224.

MacDonald DB, Al Zayed Z, Stigsby B. Tibial somatosensory evoked potential intraoperative monitoring: recommendations based on signal to noise ratio analysis of popliteal fossa, optimized P37, standard P37, and P31 potentials. *Clin Neurophysiol* 2005;116:1858–1869.

Moore B. Principal component analysis in linear systems: controllability, observability, and model reduction. *IEEE Trans Automatic Control* 1981;26:17–32.

Noss RS, Boles CD, Yingling CD. Steady-state analysis of somatosensory evoked potentials. *Electroencephalogr Clin Neurophysiol* 1996;100:453–461.

Porcaro C, Coppola G, Di Lorenzo G, et al. Hand somatosensory subcortical and cortical sources assessed by functional source separation: an EEG study. *Human Brain Mapping* 2009;30:660–674.

Regan D. *Human brain electrophysiology: evoked potentials and evoked magnetic fields in science and medicine*. New York: Elsevier Science Publishing, 1990.

Simpson DM, Tierra-Criollo CJ, Leite RT, et al. Objective response detection in an electroencephalogram during somatosensory stimulation. *Ann Biomed Eng* 2000;28:691–698.

Smith WD. Walsh versus Fourier estimators of the EEG power spectrum. *IEEE Trans Biomed Eng* 1981;28:790–793.

Suter CM. Principal component analysis of average evoked potentials. *Exp Neurol* 1970;29:317–327.

Taylor B, Gordiev K, OBrien R. In: Jones SS, Boyd S, Hetreed M, Smith N, eds. *Handbook of spinal cord monitoring: proceedings of the Fifth International Symposium on Spinal Cord Monitoring, London, UK, June 2-5, 1992*. Springer, 1994:231.

AQ : 4

Tito M, Cabrerizo M, Ayala M, et al. A comparative study of intracranial EEG files using nonlinear classification methods. *Ann Biomed Eng* 2010;38: 187–199.

Tong L, Soon VC, Huang YF, Liu R. AMUSE: a new blind identification algorithm. In: Proceedings of the IEEE International Symposium on Circuits and Systems. IEEE, 1990:1784–1787.

Tong L, Liu R-W, Soon VC, Huang Y- F. Indeterminacy and identifiability of blind identification. *IEEE Trans Circuits Sys* 1991;38:499–509.

Truccolo W, Knuth KH, Shah A, et al. Estimation of single-trial multicomponent ERPs: differentially variable component analysis (dVCA). *Biol Cybern* 2003; 89:426–438.

Weide BW, Andrews LT, Iannone AM. Real-time analysis of EEG using Walsh transforms. *Comput Biol Med* 1978;8:255–263.

Zhang XS, Roy RJ, Schwender D, Daunderer M. Discrimination of anesthetic states using mid-latency auditory evoked potential and artificial neural networks. *Ann Biomed Engineering* 2001;29:446–453.

